Technical Notes

TECHNICAL NOTES are short manuscripts describing new developments or important results of a preliminary nature. These Notes cannot exceed 6 manuscript pages and 3 figures; a page of text may be substituted for a figure and vice versa. After informal review by the editors, they may be published within a few months of the date of receipt. Style requirements are the same as for regular contributions (see inside back cover).

Hypersonic Viscous Slip Flow over an Insulated Flat Plate with Real Gas Effects

A. SUGAVANAM* AND M. S. SASTRY†
Space Science and Technology Centre, Trivandrum, India

Nomenclature

C = $\mu_w T_\infty/\mu_\infty T_w$
C_a = the mass fraction
C_p = the specific heat at constant pressure
D = dissociation energy
h = specific enthalpy
H = total enthalpy
k = Boltzmann's constant
Le = Lewis number
M = Mach number
p = pressure
p_δ^* = p_δ/p_∞, pressure ratio
Pr = Prandtl's number
$\bar{R}$ = universal gas constant
Rex = $U_\infty \rho_\infty x/\mu_\infty$, Reynolds number
T = temperature
T_D = dissociation temperature
$\bar{y}$ = y/δ, the nondimensional y coordinate
u = the velocity in x-direction
v = the velocity in y-direction
Wm = molecular weight
γ = ratio of specific heats
δ = boundary layer thickness
ρ = density
ρ_D = dissociation density
λ = mean free path
τ = shear stress
μ = coefficient of viscosity
$\bar{\chi}$ = $M_\infty^3(c/Rex)^{1/2}$, strong interaction parameter

Subscripts

∞ = conditions in freestream
δ = conditions at the edge of the boundary layer
w = conditions at the wall

Introduction

THE hypersonic boundary-layer problem is solved here for an insulated flat plate with slip effects for an ideally dissociating gas under equilibrium conditions. Kumar and Jain[1] have studied the problem without real gas effects. In Ref. 1 the term $C_1\lambda_w/L(d\eta/d\xi)^2$ is treated as a constant parameter, and consequently η was shown to be proportional to ξ. In this analysis no such parametric treatment is assumed. The problem is solved as in Refs. 1 and 3, and it is found that, apart from the real gas effects, for really small slip effects, η is still proportional to $\xi^{3/4}$ (neglecting higher order effects) for $C_1\lambda_w/\delta < 1$ (small mean free path). On the other hand, when $\delta/C_1\lambda_w$ was treated as small with higher order effects neglected (large mean free path), it was found that η is proportional to ξ. This change in the analysis clearly reveals how the mean free paths and the resulting slip effects change the character of the zero-slip strong interaction zone, where it is well known that η is proportional to $\xi^{3/4}$. Further, the series solution in terms of the slip parameter results in the slip effects' giving a negative contribution to η, thus reducing the surface pressures. For simplicity the computations are carried out for nitrogen.

Received May 16, 1973; revision received May 28, 1974.
Index category: Supersonic and Hypersonic Flow.

* Engineer, Aerodynamics Division. Presently Graduate Student, Georgia Institute of Technology, Atlanta, Ga.
† Scientific Officer, Aerodynamics Division.

Analysis

The equations of motion are

$$\partial(\rho u)/\partial x+\partial(\rho v)/\partial y = 0 \tag{1}$$

$$\rho u\frac{\partial u}{\partial x}+\rho v\frac{\partial u}{\partial y} = -\frac{\partial p}{\partial x}+\frac{\partial}{\partial y}\left(\mu\frac{\partial u}{\partial y}\right) \tag{2}$$

$$\rho u\frac{\partial H}{\partial x}+\rho v\frac{\partial H}{\partial y} = \frac{\partial}{\partial y}\left[\frac{\mu}{Pr}\frac{\partial H}{\partial y}\right]+\frac{\partial}{\partial y}\left[(Pr-1)\frac{\partial}{\partial y}\left(\frac{u^2}{2}\right)\right]-\frac{\partial}{\partial y}\left[\frac{Dk}{C_p}(Le-1)\frac{\partial C_a}{\partial y}\right] \tag{3}$$

$$p/\rho = (\bar{R}T/Wm)(1+C_a) \tag{4}$$

and for an ideally dissociating gas[2]

$$C_a^2/(1-C_a) = (\rho_D/\rho)\exp(-T_D/T) \tag{5}$$

and

$$h = (4+C_a)(\bar{R}T/Wm)+C_aD \tag{6}$$

The viscosity temperature relation is assumed as

$$\mu\alpha T^n \tag{7}$$

where $n = 0.76$. The boundary conditions are

$$y = 0, \quad v = 0, \quad u = u_v = C_1\lambda_w(\partial u/\partial y)_w \tag{8}$$

where

$$C_1 \simeq (\pi/2)^{1/2} \quad \text{and} \quad \lambda_w = 1.256\gamma^{1/2}\mu_w/a_w\rho_w$$
$$y = \delta, \quad u = u_\delta, \quad \text{and} \quad T = T_\delta$$

For $Pr = 1$ and $Le = 1$, the solution for the energy equation for an insulated flat plate is

$$h/h_\delta \simeq \tfrac{1}{2}(\gamma-1)M_\delta^2[(1-u^2/u_\delta^2)] \tag{9}$$

A linear velocity profile with slip conditions is given by

$$u/u_\delta = A+By/\delta \tag{10}$$

where

$$A = C_1\lambda_w/1+C_1\lambda_w/\delta \quad \text{and} \quad B = 1/1+C_1\lambda_w/\delta$$

With Eqs. (1) and (2), the momentum integral equation can be written as

$$\frac{\tau_w}{\rho_\infty u_\infty^2} = -\frac{p_\infty\delta}{\rho_\infty u_\infty^2}\frac{dp_\delta^*}{dx}-\frac{d}{dx}\left[\frac{\rho_\delta u_\delta^2}{\rho_\infty u_\infty^2}\int_0^\delta\frac{\rho u}{\rho_\delta u_\delta}\left(\frac{u}{u_\delta}-1\right)dy\right] \tag{11}$$

Introducing nondimensional variables,

$$\xi = x/L, \quad \eta = \delta/L$$

where $L = M_\infty^2\mu_w/\rho_\infty u_\infty$. Equation (11) reduces to

$$\frac{\tau_w}{\rho_\infty u_\infty^2} = -\frac{\eta}{\gamma M_\infty^2}\frac{dp_\delta^*}{d\xi}+\frac{2}{\gamma M_\infty^2}\frac{d}{d\xi}[p_\delta^*\eta m] \tag{12}$$

where m is defined differently for the weak and strong slip cases below.

The inviscid surface pressure distribution is computed from the tangent wedge theory as,

$$p_\delta^* = 1+\frac{\gamma(\gamma+1)}{2}M_\infty^2\left(\frac{d\eta}{d\xi}\right)^2 \tag{13}$$

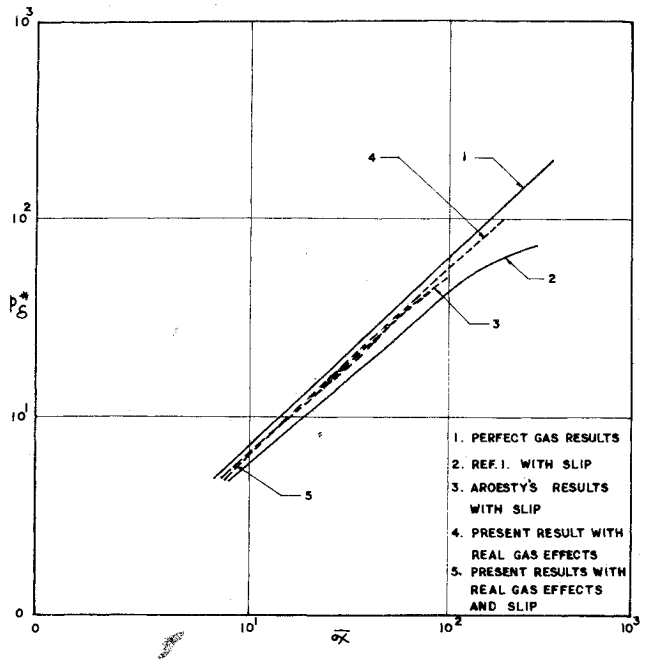

Fig. 1 Variation of p_δ^* with $\bar{\chi}$ ($M_\infty = 10$).

Case of Weak Slip

Here $\lambda_s \ll \eta$ which means $C_1\lambda_w \ll \delta$, where $\lambda_s = C_1\lambda_w/L$. For this case

$$m = \int_0^1 \frac{4+C_a}{1+C_a}\frac{1}{1-(C_aD/h)}\left(1-\frac{1}{1+\bar{y}}+\frac{\lambda_s}{\eta}\frac{1-\bar{y}}{(1+\bar{y})^2}\right)d\bar{y}$$
$$= A_1 + B_1\frac{\lambda_s}{\eta}$$

Defining $\alpha = 2-(1/m)$, Eq. (12) becomes

$$p_\delta^{*\alpha-1}\gamma m\left(1-\frac{\lambda_s}{\eta}\right) = \frac{d}{d\xi}(m^2\eta^2 p_\delta^{*\alpha}) \tag{14}$$

Expanding η (for $\alpha \simeq 1$), as in Ref. 3,

$$\eta = \eta_0 + \lambda_s\eta_1 + \cdots \tag{15}$$

For small λ_s, the zeroth-order and first-order differential equations from Eq. (14) can be obtained as

$$\gamma/A_1 = (d/d\xi)(p_\delta^*\eta_0^2) \tag{16}$$

and

$$\frac{\gamma(B_1-A_1)}{\eta_0} = \frac{d}{d\xi}\left[2A_1\eta_0(A_1\eta_1+B_1)+A_1\eta_0(A_1\eta_1+B_1)\gamma(\gamma+1)\times M_\infty^2\left(\frac{d\eta_0}{d\xi}\right)^2+\frac{d\eta_0}{d\xi}\frac{d\eta_1}{d\xi}\gamma(\gamma+1)M_\infty^2A_1^2\eta_0^2\right] \tag{17}$$

Zero-Order Solution

The solution to Eq. (16) with the involved singularity analysis at the origin was given by Pai[3] and can be directly taken over as

$$\eta_0 = \zeta^3\sum_{n=0}^{\infty}a_n\zeta^n \tag{18}$$

where $\zeta = \xi^{1/4}$ and

$$a_0 = \left(\frac{32}{9m_1C}\right)^{1/4} \tag{19a}$$
$$a_1 = 0 \tag{19b}$$
$$a_2 = -\left[\frac{m_1}{288C^3}\right]^{1/2} \tag{19c}$$
$$a_3 = 0 \tag{19d}$$
$$a_4 = \frac{1}{270a_0^3}\frac{1}{C^2} \tag{19e}$$

where $C = [\gamma(\gamma+1)/2]M_\infty^2$ and $m_1 = 2A_1/\gamma$. For small ξ this solution clearly indicates that $\eta\alpha\xi^{3/4}$ only.

First-Order Solution

The first-order differential equation (17) was first solved with $\eta_0 = a_0\xi^3$ only, and later this first-order solution was used as an initial condition to solve Eq. (17) completely for all ξ by the numerical method. This was done not only to ease the calculations but also to get a clear physical insight for η_1. The solution obtained for η_1 for small ξ is

$$\eta_1 = -\tfrac{8}{9}(\gamma-1)/A_1(1/Ca_0^4) \tag{20}$$

which shows η_1 is constant not only initially for small ξ but also negative, indicating the behavior of slip effects. Now with the complete solution of η_0, as given by relation (19), and the initial η_1 for small ξ, as in Eq. (20), the differential equation in (17) can be solved completely by a Runge-Kutta procedure.

Strong Slip Case

Here $\eta/\lambda_s \ll 1$. In this case

$$m = \frac{1}{2}\int_0^1 \frac{4+C_a}{1+C_a}\frac{1}{1-(C_aD/h)}\left[1+\frac{\eta}{2\lambda_s}(\bar{y}-1)\right]d\bar{y}$$
$$= A_2 + B_2\eta/\lambda_s$$

For this case the momentum integral equation can be derived as

$$\frac{\gamma}{\lambda_s} = -\eta\frac{dp_\delta^*}{d\xi}+\frac{d}{d\xi}[\eta p_\delta^*(A_2+B_2\eta(\lambda_s)] \tag{22}$$

with $\eta/\lambda_s d\eta/d\xi \simeq 0$ for small ξ and $\alpha = 1$. Equation (22) can be solved as

$$\eta = \left[\frac{2}{\lambda_s A_2(\gamma+1)M_\infty^2}\right]^{1/3}\xi \tag{23}$$

It may be mentioned that α in this case is really not of order unity. However, for better accuracy, Eq. (22) itself can be solved with a series solution of the form

$$\eta = \sum_{n=1}^{\infty}a_n\xi^n \tag{24}$$

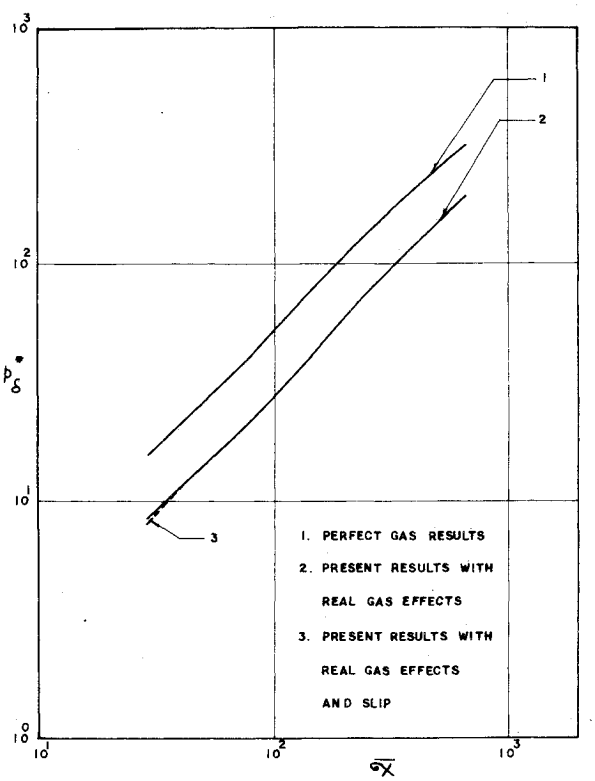

Fig. 2 Variation of p_δ^* with $\bar{\chi}$ ($M_\infty = 20$).

Conclusions

The graphs in Fig. 1 are for p_b* vs $\bar{\chi}$ at Mach number 10. Curves 1, 4, and 5 present the calculations of this report for the perfect gas case, the real gas case with no slip effects, and the real case with slip effects. Curve 4, when compared with curve 1, indicates that the real gas effects are not very significant for the Mach number considered, which is also obvious and expected because T_{aw} is only around 4000°K. This analysis also is useful and presents a method of solving for the real gas effects with slip for the regime between the strong interaction zone and the strong slip zone, where the behavior of η with respect to ξ should be of the strong interaction zone itself for continuity purposes. Again the reduction of the boundary-layer growth due to slip effects is clearly brought out by the first-order solution. The results for the strong slip can be obtained in a similar manner.

To conclude, the small slip effects do not really change the character of η with respect to ξ, which changes only when the strong slip effects are present. The Aroesty[4] first-order results are in good agreement with the present results, indicating that his results are only for the weak slip case and for this reason the results of Kumar and Jain[1] for the strong slip are not in agreement with Aroesty's results. Real gas effects are not very significant in the Mach number 10 case, but are seen to be dominant for the Mach number 20 case as in Fig. 2.

References

[1] Kumar, A. and Jain, A. C., "Hypersonic Viscous Slip Flow over Insulated Wedges," *AIAA Journal*, Vol. 10, No. 8, Aug. 1972, pp. 1081–1083.

[2] Lighthill, M. J., "Dynamics of a Dissociating Gas," *Journal of Fluid Mechanics*, Vol. 2, Pt. 1, Jan. 1957, pp. 1–32.

[3] Pai, S. I., "Hypersonic Viscous Flow over an Insulated Wedge at an Angle of Attack," TN BN42, Inst. for Fluid Dynamics and Applied Mathematics, University of Maryland, Baltimore, 1954.

[4] Aroesty, J., "Slip Flow and Hypersonic Boundary Layers," *AIAA Journal*, Vol. 2, No. 1, Jan. 1964, pp. 189–190.

Transient Eigenfrequencies in Liquid-Filled Cylinders

ANDREW MARK*
U.S. Army Ballistic Research Laboratories, Aberdeen Proving Ground, Md.

Introduction

THE motion of liquids in rotating containers is of interest to geophysicists because of the terrestrial molten core theory and to aerospace scientists and ballisticians because liquid payloads in missiles and projectiles can present a variety of complicated flight anomalies. In many of the past investigations on this subject, the liquid motion has been the primary concern and the liquid-container interaction was not always considered.

The Ballistic Research Laboratories study the behavior of cannon-launched, liquid-filled projectiles where the total system is of interest. The liquid is contained in a right circular cylinder within the projectile. Upon launch from a cannon, the casing (cylinder) is brought to a large, finite spin in a short time and is then acted upon by liquid and aerodynamic forces, both tending to decrease casing spin. If the projectile casing nutational frequency is sufficiently close to a liquid eigenfrequency, the possibility of resonance and resulting yaw amplification exists. This type of instability can occur while the liquid is in rigid body rotation or when the liquid is spinning up.

It was the objective of this undertaking to obtain experimental evidence of projectile instability during this spin-up phase (transient instability) and to infer increase in liquid angular momentum by measuring projectile casing spin decay. This was accomplished by the use of solar aspect sensors and radar tracking. Projectiles serve as convenient vessels when studying liquid spin-up and instability under large, impulsive, axial spins and in no way detract from their results to be generally applicable to cylindrical containers.

The solar aspect sensors consist essentially of photovoltaic cells placed behind slits in the ogive portion of the projectile. The slits are oriented such that the spinning and yawing motion of the projectile may be extracted from a series of pulses produced by the cells as they sweep past the sun. The pulses are telemetered to ground and recorded on magnetic tape. Details of the technique in accomplishing the measurements are presented in Refs. 1–3.

Five liquid-filled projectiles were fired from a 155 mm gun with a muzzle velocity of 1032 ± 15 fps generating an initial spin rate of 625 ± 9 sec^{-1} and having a nominal 30 sec flight time. Three of the projectiles, with a cavity length to diameter ratio (c/a) of 4.39, were filled to 90% of their volume with water while the remaining two with a cavity length to diameter ratio of 4.90 were filled to 80%. The cavity dimensions and fill ratios were chosen because past experience dictated a stable flight for the 90% filled case and an unstable one for the 80% case.

Redundancy of experiment is dictated whenever gun launched telemetering is involved and only a sample of each case is presented here.

Spin-Up

The casing of a liquid-filled projectile is subjected to two axially oriented moments; one of liquid origin (internal) and the other aerodynamic (external). We may therefore write the conservation of angular momentum about the axial direction as

$$M_{\text{aero}} + M_{\text{liq}} = -I_a \dot{p} \tag{1}$$

where I_a is the axial moment of inertia of the casing and $\dot{p}$ is the rate of change of casing spin. After substituting the relationship for the aerodynamic moment

$$M_{\text{aero}} = \tfrac{1}{2} C_{l_p} \rho V S l^2 p \tag{2}$$

integrating and manipulating terms we obtain

$$\frac{L_{\text{liq}}}{L_{\text{liq (rigid)}}} = \frac{I_a}{I_{\text{liq}}}\left(\frac{p_0}{p} - 1\right) - \frac{Sl^2 \int_0^t (\rho V C_{l_p} p)\, d\tau}{2 I_{\text{liq}}\, p} \tag{3}$$

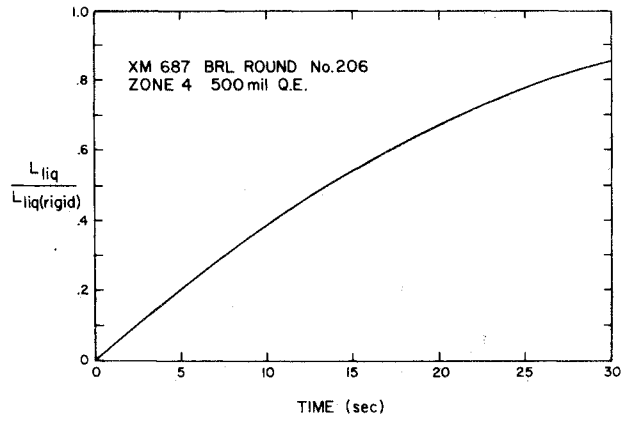

Fig. 1 Temporal increase in angular momentum of a liquid contained in a projectile.

Received February 6, 1974; revision received May 28, 1974.
Index categories: Hydrodynamics; Wave Motion and Sloshing.
* Aerospace Engineer. Member AIAA.